Hindawi Publishing Corporation
Science and Technology of Nuclear Installations
Volume 2008, Article ID 428168, 18 pages
doi:10.1155/2008/428168

Research Article

SBWR Model for Steady-State and Transient Analysis

Gilberto Espinosa-Paredes[1] and Alejandro Nuñez-Carrera[2]

[1] *Area de Ingeniería en Recursos Energéticos, Universidad Autónoma Metropolitana-Iztapalapa, Avenida San Rafael Atlixco 186, Colonia Vicentina, 09340 México DF, Mexico*
[2] *Comisión Nacional de Seguridad Nuclear y Salvaguardias, Avenida Doctor Barragán 779, Colonia Vicentina, 03020 México DF, Mexico*

Correspondence should be addressed to Gilberto Espinosa-Paredes, gepe@xanum.uam.mx

Received 13 December 2007; Accepted 21 February 2008

Recommended by Dilip Saha

This paper presents a model of a simplified boiling water reactor (SBWR) to analyze the steady-state and transient behavior. The SBWR model is based on approximations of lumped and distributed parameters to consider neutronics and natural circulation processes. The main components of the model are vessel dome, downcomer, lower plenum, core (channel and fuel), upper plenum, pressure, and level controls. Further consideration of the model is the natural circulation path in the internal circuit of the reactor, which governs the safety performance of the SBWR. To demonstrate the applicability of the model, the predictions were compared with plant data, manufacturer_s predictions, and RELAP5 under steady-state and transient conditions of a typical BWR. In steady-state conditions, the profiles of the main variables of the SBWR core such as superficial velocity, void fraction, temperatures, and convective heat transfer coefficient are presented and analyzed. The transient behavior of SBWR was analyzed during the closure of all main steam line isolation valves (MSIVs). Our results in this transient show that the cooling system due to natural circulation in the SBWR is around 70% of the rated core flow. According to the results shown here, one of the main conclusions of this work is that the simplified model could be very helpful in the licensing process.

1. INTRODUCTION

Recently, a joint project among three Agencies: the International Energy Agency (IEA), the OECD Nuclear Energy Agency (NEA), and the International Atomic Energy Agency (IAEA) prepared the report "Innovative nuclear reactor development, opportunities for International cooperation" [1], whose main objective is the identification of opportunities to establish joint projects in developing nuclear fission reactor technologies. This study remarks that the following areas are good candidates for developing new, broad based collaborative efforts:

(i) natural circulation;
(ii) high-temperature materials;
(iii) passive (safety) devices;
(iv) in-service inspection and maintenancemethods;
(v) advanced monitoring and control technologies;
(vi) delivery and construction methods;
(vii) safeguard technologies and approaches.

This paper focuses on the attention in natural circulation which is one of the good candidates for developing new reactor technologies. Natural convection circulation of coolant in the reactor cooling system is used to some extent in all reactor concepts, and many of these uses are innovative [2]. What is now needed is to develop or confirm the design basis and to develop and qualify computer codes to enable reliable analysis.

All the ordinary water-cooled and heavy water-cooled reactor designs rely on natural convection of the coolant to remove decay heat from the fuel after shutdown, even today's operating water reactors also rely on natural convection to remove decay heat when forced circulation is lost.

Among the new design with natural circulation, we can mention the CAREM-25 [3] and NHR-200 [4], both use

natural convection circulation of the ordinary water coolant at all power levels to remove heat from the reactor core. The energy amplifier and BREST 300 [5] use natural circulation of the lead coolant to remove decay heat from the core after shutdown, requiring the design of a reliable system to accommodate the potential solidification of the lead in regions outside the core. The energy amplifier also uses natural circulation of the coolant to remove heat produced by fission from the reactor core at all power levels; it is important to remark that this has not been done before. The FUJI [2] uses natural circulation of the molten salt reactor coolant to remove decay heat from the core after shutdown. Therefore, the ability to predict the performance of systems operating in natural convection circulation mode has fundamental importance.

One of the main design concepts is presently proposed by general electric (GE): the simplified boiling water reactor (SBWR) [6] and the economic and simplified boiling water reactor (ESBWR) [7]. According to the manufacturer, these new design reactors working with natural circulation provide simplification over previous BWRs. The improvements are accomplished by the removal of the recirculation pumps and associated motors, piping, valves, heat exchanges, control, and electrical support systems that exist with forced recirculation, eliminating flow disturbance by abnormal pump behavior. The main differences between natural and forced circulations are the additions of an exhaust pipe above the reactor core to stabilize and direct the steam and water flow above the core, and the correspondingly open and downcomer annulus that reduces the flow resistance and provides additional driving head pushing the water to the bottom of the core. Among the benefits of these designs are simplification of the operation, higher plant availability, 20% reduction in the cost of operation and maintenance, and the reduction of personnel dose by the elimination of recirculation pumps maintenance.

Simplified and convenient models are used in computer codes to perform analysis in early stages of the design of experimental reactor facilities and Generation IV reactors. The work of Tian et al. [8] showed a simplified neutronic and thermalhydraulic model used in the China Advanced Research Reactor (CARR) and its application with a simulation of loss of power accident without emergency cooling system. Other application is the engineering safety analysis for regulatory licensing process of light water reactors (LWR) that were performed in the past using simplified one-dimensional models of thermalhydraulics systems with the appropriate initial and boundary conditions for transient analysis in two-phase flow phenomena due that it can provide overestimated results.

This paper presents an SBWR model for transient analysis, where the thermalhydraulic model that describes the dynamic behavior of the lower and upper plena, and the reactor core, as well as fuel temperature model were based on distributed parameter approximations. The vessel dome, downcomers, recirculation loops, and neutron process models were based on lumped parameter approximations.

A multinode fuel pin model is developed to describe the heat transfer process. Three regions were identified as indispensable to be considered in the heat transfer analysis: the first region corresponds to heat transfer in the fuel; the second region corresponds to heat transfer in the gap; and the third region corresponds to heat transfer in the clad, whose temperatures are determined by the rate of heat convection due to core flow.

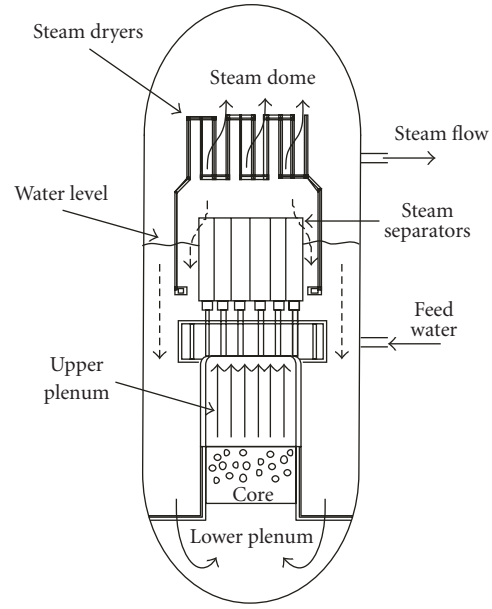

Figure 1: SBWR configuration and flow paths.

Reactor power is calculated from a point reactor kinetics model with six groups of delayed neutrons. The reactivity due to Doppler effect, void fraction, moderator temperature, and control rod drive was considered in this model.

This paper is organized as follows. The SBWR system description is presented in Section 2; mathematical models are described in Section 3; and Section 4 shows the results and discussions. The qualification assessment is presented in the appendix.

2. SYSTEM DESCRIPTION

The SBWR configuration and the flow paths are illustrated in Figure 1. The reactor natural circulation loop circulates the required coolant flow through the reactor core. The flow within the reactor vessel provides a continuous internal natural circulation path for a major portion of the core coolant flow. The core flow is taken from the vessel and discharged into the lower core plenum. The coolant water passes along the individual fuel rods inside the fuel channel where it boils and becomes a two-phase steam/water mixture. In the core, the two-phase fluid generates upward flow through the axial steam separators, while the steam continues through the dryers and flows directly out through the steam lines into the turbine generator. The condensate flow is then returned through the feed water heaters by the condensate feed water pumps into the vessel. Finally, the water, which is separated from the steam in the steam separators, flows

Table 1: Nominal parameters for SBWR [9].

Parameter	Units
Thermal power	1800 MWth
Total inlet core flow	6666 kg/sec
Pressure at the dome of vessel	7.07 MPa
Total steam flow	1100 kg/sec
Feed water temperature	488 K
Active fuel length	2.74 m
Pressure vessel internal height	22 m

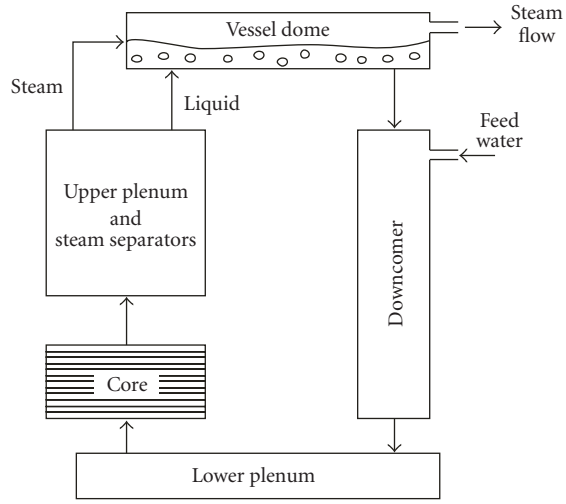

Figure 2: Schematic diagram of the SBWR.

downward in the periphery of the reactor vessel and mixes with the incoming main feed flow from the turbine.

Table 1 shows the nominal values used in the simulation, which correspond to design characteristics of the SBWR [9].

3. MATHEMATICAL MODEL

Figure 2 is a schematic diagram of the SBWR where the arrangement of the computational cells of the SBWR model is shown. The reactor vessel was divided into five zones. Two of these zones, the vessel dome and the downcomer, have variable volume according to the vessel water level. The three fixed volume zones are the lower plenum, the upper plenum and steam separators, and the reactor core. Due to its importance on the model performance, the latter was subdivided into twelve one-dimensional nodes. The reactor model is completed by including natural recirculation loop as coolant, neutron kinetics, fuel rod temperature, and control models. In addition, this model uses a set of empirical correlations valid for the normal range of SBWR operating conditions. The model derivation is based in lumped and distributed parameters approximation; Table 2 presents the submodels and approximations used.

Table 2: SBWR submodels and approximations.

Mode*l	Approximation
Vessel dome and downcomer	Lumped parameters
Natural circulation loop	Lumped parameters
Neutron kinetics	Lumped parameters
Fuel rod	Distributed parameters
Lower plenum, upper plenum, and core	Distributed parameters

* The whole system includes pressure control and level control.

The following assumptions were adopted in the development of the SBWR model:

(i) the point-kinetic equations are used to describe the evolution of neutron population and precursor concentration;

(ii) delayed neutrons are modeled using six groups;

(iii) fuel rod is described by a distributed parameters model, which includes fuel, gap, and cladding. This model is crucial due that velocity of heat transfer from fuel to the coolant has important impact during transient behavior;

(iv) the multiple parallel channels in SBWR are lumped into one average channel. The drift-flux model is used to consider velocity difference between liquid and vapor phases;

(v) the axial power profile is modeled as a superposition of a profile space-dependent and a space-independent term, that is, time-dependent;

(vi) the downcomer section is assumed to be filled with single-phase fluid. The thermohydraulics system itself consists of five different sections: lower plenum, core, upper plenum, stem separators, and downcomer. The heated section is the core, and the others are unheated sections;

(vii) the gas phase is saturated at the vessel pressure.

3.1. Thermalhydraulic model

The thermalhydraulic model consists of five balance equations: (1) liquid-and gas-phase mass balances, (2) mixture momentum, (3) mixture energy, (4) liquid-phase energy, together with a drift flux approach [10], for the analysis of phase separation. The nonequilibrium two-phase flow for the volumetric vapor generation rate in subcooled boiling was considered using Saha and Zuber approximation [11, 12].

Nonequilibrium two-phase flow conditions are present in all two-phase flows, and the effects of nonequilibrium states can be important at steady-state and off-normal conditions encountered in operational transients. In boiling water reactor, for example, vapor voids are formed in the core when the bulk liquid is below the saturation state; this phenomena is known as subcooled boiling. These voids have a very strong effect relative to the power distribution in the

core both at quasi-steady conditions and during operational transient.

The thermalhydraulic model is used to describe the dynamic behavior of the lower and upper plena, downcomer, and the reactor core. The five-equation model was based on the following assumptions: (i) one-dimensional flow, (ii) no cross flow, and (iii) kinetic and potential energy effects are neglected in the energy equation.

The model is based on liquid- (denoted by subscript l) and gas- (denoted by subscript g) phase mass and energy balances, and a mixture momentum balance (denoted by subscript m):

$$\begin{aligned}\frac{\partial}{\partial t}(\rho_g\varepsilon_g)+\frac{\partial}{\partial z}(j_g\rho_g)&=\Gamma,\\ \frac{\partial}{\partial t}(\rho_l\varepsilon_l)+\frac{\partial}{\partial z}(j_l\rho_l)&=-\Gamma,\end{aligned}\tag{1}$$

$$\frac{\partial}{\partial t}(\rho_l h_l\varepsilon_l)-\varepsilon_l\frac{\partial p}{\partial t}+\frac{\partial}{\partial z}(\rho_l h_l j_l)=\frac{q''_l P_H}{A_{x-s}}+q'''_l\,\varepsilon_l-\Gamma h_f,\tag{2}$$

$$\frac{\partial}{\partial t}(\rho_m h_m)-\frac{\partial p}{\partial t}+G_m\frac{\partial h_m}{\partial z}=\frac{q''P_H}{A_{x-s}}+q''',\tag{3}$$

$$\frac{\partial G_m}{\partial t}+\frac{\partial}{\partial z}\left(\frac{G_m^2}{\rho_m}\right)=-\frac{\partial p}{\partial z}-\frac{f\,G_m^2}{2\rho_m D_h}-g\rho_m,\tag{4}$$

where

$$\rho_m=\rho_g\varepsilon_g+\rho_l\varepsilon_l,\tag{5}$$

$$\rho_m h_m=\rho_g h_g\varepsilon_g+\rho_l h_l\varepsilon_l,\tag{6}$$

$$G_m=\rho_g j_g+\rho_l j_l,\tag{7}$$

$$\varepsilon_g+\varepsilon_l=1.\tag{8}$$

In these equations, ρ is density, ε_g is the void fraction; j is superficial velocity; Γ is the volumetric vapor generation rate; h is the enthalpy; p is the pressure; q'' is the heat flux; P_H is the heated perimeter; A_{x-s} is the cross-sectional area; f is the friction factor; D_h is the hydraulic diameter; and q''' is the volumetric heat generation by gamma radiation. For unheated sections (e.g., downcomer, lower and upper plenums) $q''=0$.

The equations of state are usually expressed in terms of two independent variables in the form $\rho_l=\rho_l(p,h_l)$ for density and $T_l=T_l(p,h_l)$ for temperature. If the fluid is at the saturation state, the state properties are functions of the pressure only, and the equations of state can be written as $\rho_k=\rho_k(p)$ to density and $T_k=T_k(p)$ where $k=l$ or g. For the gas phase and in all cases $h_g=h_g(p)$.

Depending on the mixture enthalpy h_m, the following two cases were considered.

Case 1. If $h_f(p)<h_m<h_g(p)$, the gas and liquid phases are saturated at reactor pressure and $h_l=h_f(p)$.

Case 2. If $h_m<h_f$ and $h_l<h_f$, liquid phase occurs first and, subsequently, subcooled boiling appears.

Here, h_f and h_g are the enthalpy of liquid and vapor saturated at the vessel pressure, respectively.

For bulk boiling condition, both the gas and liquid phases are in saturated condition (thermodynamic equilibrium condition) at the vessel pressure, then if $h_l=h_f(p)$; $\rho_l=\rho_f(p)$ in (3) and combining it with (1), the volumetric vapor generation rate Γ is given by:

$$\Gamma=\frac{1}{h_{fg}}\left[\frac{q''P_H}{A_{x-s}}+q'''+\left(1-\rho_g\varepsilon_g\frac{\partial h_g}{\partial p}-\rho_f\varepsilon_l\frac{\partial h_f}{\partial p}\right)\frac{\partial p}{\partial t}-\rho_f j_l\frac{\partial h_f}{\partial z}\right].\tag{9}$$

In these equations, $\partial h_g/\partial z=0$, due that the gas phase is saturated at the vessel pressure, h_{fg} is the difference in specific enthalpy of saturated vapor and liquid. For subcooled boiling, the volumetric vapor generation is given by [11]:

$$\Gamma=\frac{1}{h_{fg}}\left[\frac{q''P_H}{A_{x-s}}\left(1-\frac{h_f-h_l}{h_f-h_{ld}}\right)+q'''-H_o\frac{h_{fg}}{\nu_{fg}}\varepsilon_g(T_s-T_l)+\varepsilon_g\left(1-\rho_g\frac{\partial h_g}{\partial p}\right)\frac{\partial p}{\partial t}\right],\tag{10}$$

where H_o is the condensation parameter, and the liquid subcooling (h_f-h_{ld}) at the initiation of subcooled boiling is given by [12]

$$h_f-h_{ld}=\begin{cases}0.0022q''D_hCp_l/k_l, & \text{Pe}<70{,}000,\\ 154q''/G, & \text{Pe}>70{,}000.\end{cases}\tag{11}$$

Here, k_l is the liquid thermal conductivity; Cp_l is the liquid specific heat; and T_s is the saturation temperature.

The mass flow rate of each phase is, respectively, given by

$$\begin{aligned}W_g&=j_gA_{x-s}\rho_g,\\ W_l&=j_lA_{x-s}\rho_l,\end{aligned}\tag{12}$$

where $j_l=j-j_g$. In order to calculate the amount of steam and liquid from mixture properties, the drift-flux model was used [10]. This model provides an algebraic relationship between the relative velocities of the flowing liquid and steam and the void fraction. The basic equation of the drift flux model is as follows:

$$j_g=(C_oj+\nu_{gj})\varepsilon_g.\tag{13}$$

The distribution parameter C_o and the average drift velocity ν_{gj} are represented by a correlation for each of the two-phase flow regimes, bubbly and slug in the present case, in vertical pipes. The superficial velocity is calculated by:

$$j=\left[\left(\frac{1}{\rho_g}-\frac{1}{\rho_l}\right)\Gamma-\left(\frac{\varepsilon_g}{\rho_g}\frac{\partial\rho_g}{\partial p}+\frac{\varepsilon_l}{\rho_l}\frac{\partial\rho_l}{\partial p}\right)\frac{\partial p}{\partial t}-\xi_{\text{sub}}\right]\Delta z+\left(\frac{W_{\text{gin}}}{\rho_g}+\frac{W_{\text{lin}}}{\rho_l}\right)\frac{1}{A_{x-s}},\tag{14}$$

Table 3: Thermal hydraulics parameters.

Parameter	Value
A_{x-s}	4.024 m^{2*}
D_h	0.0152 m
C_0	1.2–0.2 $(\rho_g/\rho_l)^{0.5}$; $\varepsilon_g < 0.65$
H_0	0.24 (s$\cdot$ ^{o}K)$^{-1}$
P_H	849.57 m
v_{gj}	$1.53g^{0.2}[\sigma g(\rho_l - \rho_g)/\rho_l^2]^{0.2}$; $\varepsilon_g < 0.65$

* 516 assemblies.

where

$$\xi_{\text{sub}} = \begin{cases} \dfrac{\varepsilon_l}{\rho_l}\left(\dfrac{\partial \rho_l}{\partial h_l}\right)\dfrac{\partial h_l}{\partial t}, & \text{Subcooled boiling,} \\ 0, & \text{Thermodynamic equilibrium.} \end{cases} \tag{15}$$

Here, Δz is the cell length in axial direction; W_{gin} and W_{lin} are the inlet mass flow rate of the gas and liquid phases, respectively.

Equations (1)–(15) represent the thermalhydraulic model, which consider nonequilibrium two-phase flow effects and velocities difference between liquid and vapor phases. The main advantage of this model is its simplicity requiring only and few constitutive equations. In fact, only well-known, wall-to-mixture heat transfer and friction constitutive relationships are required. The term $\partial p/\partial t$ in the equations of the thermalhydraulic model corresponds to vessel dome, which is presented in Section 3.5 The thermalhydraulic parameters are presented in Table 3.

For time discretization, an explicit Euler method was used, with a fixed time step of 0.01 second to solve the equations set of the thermalhydraulic models. This time step is highly recommended for transient with fast change in vessel pressure. Regarding the spatial discretization, the scheme used is known as a first-order, upwind finite difference scheme with a truncation error of order Δz.

3.2. Reactor power model

The reactor power is given by

$$P(t,z) = n(t)F(z)P_0, \tag{16}$$

where $F(z)$ is the axial power factor (which is given by Figure 3); P_0 is nominal power; and $n(t)$ is the normalized neutron flux, which is calculated from a point reactor kinetics model with six groups of delayed neutrons:

$$\frac{dn(t)}{dt} = \frac{\rho(t) - \beta}{\Lambda} n(t) + \sum_{i=1}^{6} \lambda_i c_i(t), \tag{17}$$

$$\frac{dc_i(t)}{dt} = \frac{\beta_i}{\Lambda} n(t) + \lambda_i c_i(t), \quad i = 1, 2, \ldots, 6, \tag{18}$$

where c_i is a delayed neutron concentration of the ith precursor group normalized with the steady-state neutron density; ρ is the net reactivity; β is the neutron delay fraction;

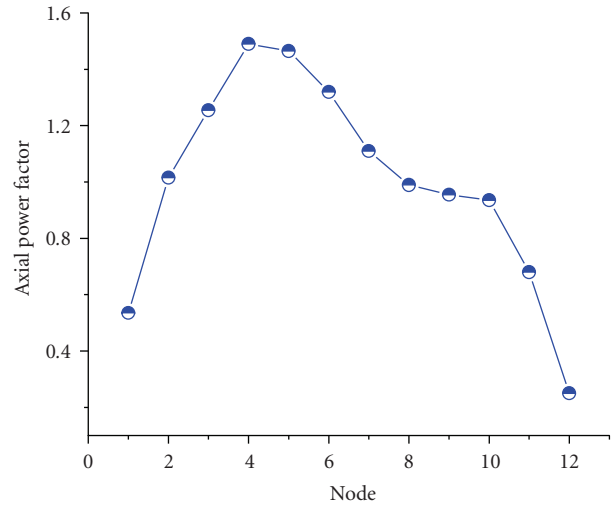

Figure 3: Axial power distribution.

Table 4: Neutron delay fraction and decay constant [13].

	β_i	λ_i
Group 1	2.470×10^{-4}	0.0127 s^{-1}
Group 2	1.355×10^{-3}	0.0317 s^{-1}
Group 3	1.222×10^{-3}	0.1150 s^{-1}
Group 4	2.646×10^{-3}	0.3110 s^{-1}
Group 5	8.320×10^{-4}	1.4000 s^{-1}
Group 6	1.690×10^{-4}	3.8700 s^{-1}
β	6.5×10^{-3}	
Λ	4.0×10^{-5} s^{-1}	

Λ is the neutron generation time; and β_i is the portion of neutrons generated by the ith group. The initial conditions are given by $n(0) = n_0$ and $c_i(0) = \beta_i n_0/\Lambda\lambda_i$. The parameters of the kinetics model are presented in Table 4.

The net reactivity of the nuclear reactor includes four main components: feedback reactivity due to the void fraction in the two-phase flow ρ_v, Doppler effect ρ_D due to fuel temperature, moderator temperature ρ_m, and reactor control rods ρ_{cr}. Therefore, we express the feedback reactivities as:

$$\rho(t) = \rho_v(t) + \rho_D(t) + \rho_m(t) + \rho_{\text{cr}}(t). \tag{19}$$

The kinetics point equations are stiff in the coefficients because they differ in several orders of magnitude, especially in (17). The variable implicit integration method [14] was used to solve (17), and the Euler method in an explicit form was used to solve the delayed precursor concentration given by (18). The reactivity correlations are presented in Table 5.

3.3. Fuel model

The fuel assembly temperature distribution was obtained considering each radial node at each of the twelve hydraulic axial nodes in the core. Two radial nodes are considered for the clad and the gap, two more nodes for the boundary condition evaluation, and four nodes are considered for one equivalent fuel element, as illustrated in Figure 4.

Table 5: Reactivity correlations.

Reactivity (pcm)
Void fractions reactivity
$\rho_v(\langle\varepsilon_g\rangle) = -4.0925 - 41.036\langle\varepsilon_g\rangle + 30.8223\langle\varepsilon_g\rangle^2$.
Doppler effect
$\rho_D = 1.3 - 0.005\langle T_f\rangle + 2.0\times10^{-6}\langle T_f\rangle^2 + -3.0\times10^{-11}\langle T_f\rangle^3 - 1.1\times10^{-3}\langle\varepsilon_g\rangle(\langle T_f\rangle - 325.0)$.
Moderator temperature reactivity
$\rho_m = 1.656 - 1.035\times10^{-2}\langle T_m\rangle + 4.0\times10^{-5}\langle T_m\rangle^2 - 7.33\times10^{-8}\langle {T_m}^3\rangle$.
Control rod drive reactivity
$\rho_{\text{cr}} = -11.235 + \dfrac{57.73(1-\text{CRD})}{1+0.937(1-\text{CRD})}$.

A detailed multinode fuel pin model is developed for this study. The fuel heat transfer formulation is based on the following fundamental assumptions: (i) axis-symmetric radial heat transfer; (ii) the heat conduction in the axial direction is negligible in respect to the heat conduction in the radial direction; (iii) the volumetric heat rate generation in the fuel is uniform in each radial node; and (iv) storage of heat in the fuel cladding and gap is negligible.

Under these assumptions, the transient temperature distribution in the fuel pin, initial, and boundary conditions are given by:

$$(\rho Cp)\frac{\partial T}{\partial t} = k\frac{1}{r}\frac{\partial}{\partial r}\left(r\frac{\partial T}{\partial r}\right) + q'''(t), \quad \text{at } r_0 \le r \le r_6, \tag{20}$$

$$\text{I.C.} \quad T(r,0) = T(r), \quad \text{at } t = 0, \tag{21}$$

$$\text{B.C.1} \quad -k\frac{\partial T}{\partial r} = H_\infty(T - T_m), \quad \text{at } r = r_6, \tag{22}$$

$$\text{B.C.2} \quad \frac{\partial T}{\partial r} = 0, \quad \text{at } r = r_0. \tag{23}$$

In these equations, r is the cylindrical radial coordinate; r_0 and r_6 are defined in Figure 4, $q'''(t) = P(t)/V_f$ at each axial node, where P is given by (16); T_m is the moderator temperature; and H_∞ is the convective heat transfer coefficient, which is presented in Section 3.4.

In the present solutions, the fuel element is represented by a one-dimensional, mesh-centred grid consisting of a variable number of radial elements at each axial position. The differential equations described previously are transformed into discrete equations using the control volume formulation technique in an implicit form [15].

Application of the control volume formulation enables the equations for each region (fuel, gap, and clad) to be written as a single set of algebraic equations for the sweep in the radial direction:

$$a_j T_{j-1}^{t+\Delta t} + b_j T_j^{t+\Delta t} + c_j T_{i,j+1}^{t+\Delta t} = d_j, \tag{24}$$

where $T_{j-1}^{t+\Delta t}$, $T_j^{t+\Delta t}$, and $T_{j+1}^{t+\Delta t}$ are unknowns; a_j, b_j, c_j, and d_j are coefficients, which are computed at the time t.

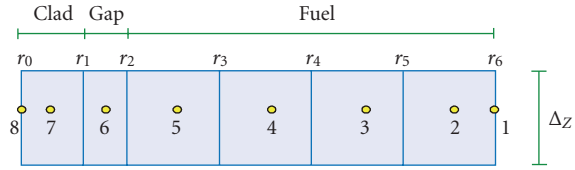

Figure 4: Arrangement of the computational cells of gap, clad, and fuel.

When these equations are put into a matrix form, the coefficient matrix is tridiagonal. The solution procedure for the tridiagonal system is the Thomas algorithm [15], which is the most efficient algorithm for this type of matrices. The coefficients a_j, b_j, c_j are dependents of thermophysical properties, that is, thermal conductivity, density, and specific heat, and since they are at function of $T_j^{t+\Delta t}$, at least one iteration is needed.

The interaction of the model with the neutron kinetics model is through evaluation of the average fuel temperature $\langle T_f\rangle$ and the volumetric heat rate generation q'''. The interaction with the nuclear thermalhydraulics is through evaluation of the coolant temperature and heat transfer coefficient. The average fuel temperature is given by:

$$\begin{aligned}\langle T_f\rangle &= \frac{1}{V_f}\int_{V_f} T_f\,dV \\ &\simeq \frac{1}{V_f}\sum_{i=1}^{n}\left(V_2T_{i,2} + V_3T_{i,3} + V_4T_{i,4} + V_5T_{i,5}\right),\end{aligned} \tag{25}$$

where $V_f = V_2 + V_3 + V_4 + V_5$ is the fuel volume. Here 2, 3, 4, and 5 represent the radial node according to Figure 4, while that i represents the axial index of the node. Fuel parameters are shown in Figure 4 and Table 6.

3.4. Convective heat transfer coefficients

The convective heat transfer coefficient for the single-phase liquid and vapor ($H_{1\phi}$) is obtained from the classical Dittus-Boelter correlation [16]. The heat transfer coefficient in both subcooled boiling and nucleate boiling regimes ($H_{2\phi}$) is calculated with the Chen correlation [17]. The convective

Table 6: Fuel model parameters [14].

Fuel

$$K_f = \frac{3825.02}{\langle T_f\rangle + 129.41} + 6.08\times 10^{-11}\langle T_f\rangle^3,\ \text{J/m·s},$$

$$(\rho Cp)_f = \frac{8.5103\times 10^{11} e^{535.28/\langle T_f\rangle}}{\langle T_f\rangle\left(e^{535.28/\langle T_f\rangle}-1\right)^2} + 2.4348\times 10^2\langle T_f\rangle + \frac{1.6609\times 10^{16} e^{-1.8970x10^4/\langle T_f\rangle}}{\langle T_f\rangle^2},\ \text{J/m}^3\text{·K},$$

$$V_f = 8.9335\,\text{m}^3.$$

Clad

$$K_{\text{cl}} = 7.51 - 0.0209T_{\text{cl}} - 1.45\times 10^{-5}T_{\text{cl}}^2 + 7.67\times 10^{-9}T_{\text{cl}}^3,\ \text{J/m·s},$$

$$(\rho Cp)_{\text{cl}} = 1.8204\times 10^6 + 3.0386\times 10^5\theta_{\text{cl}} - 1.0637\times 10^5\theta_{\text{cl}}^2 + 2.8102\times 10^4\theta_{\text{cl}}^3 + -2723.6\theta_{\text{cl}}^4,\ \text{J/m}^3\text{·K},$$

$$\theta_{\text{cl}} = \frac{T_{\text{cl}} - 300}{200}.$$

Gap

$$K_{\text{ga}} = \frac{H_{\text{gap}}}{\delta_{\text{gap}}} = \frac{2936.8}{1.14\times 10^{-4}},\ \text{J/m·s}.$$

heat transfer coefficient (H_∞) is given by the maximum between $H_{1\phi}$ and $H_{2\phi}$ to avoid discontinuities, that is, $H_\infty = \text{MAX}(H_{1\phi}, H_{2\phi})$.

The interaction of the convective heat transfer coefficients with the fuel heat transfer model is through the evaluation of the clad temperature $T|_{r=r_6}$ (Figure 4). The convective heat transfer coefficient H_∞ is used in the boundary condition given by (22).

3.5. Vessel dome model

The vessel dome is modeled as a two-region volume, one region being liquid and the other vapor. The two regions are assumed to be at the same pressure but not necessarily at the same temperature. The dynamic model used to obtain the pressure in the vessel dome is based on macroscopic balances of mass and energy:

$$\frac{dp}{dt} = -\frac{\nu_l\sum_j W_{jl} + \left(\partial\nu_l/\partial h_l\right)_p\sum_j W_{jl}\left(h_{jl}-h_l\right)}{Q+Q'} + \frac{\nu_v\sum_j W_{jv} + \left(\partial\nu_v/\partial h_v\right)_p\sum_j W_{jv}\left(h_{jv}-h_v\right)}{Q+Q'}, \tag{26}$$

where Q denotes $m_l[\nu_l(\partial\nu_l/\partial h_l)_p + (\partial\nu_l/\partial p)_{h_l}]$ and Q' denotes $m_v[\nu_v(\partial\nu_v/\partial h_v)_p + (\partial\nu_v/\partial p)_{h_v}]$, and W_{jl} and W_{jv} are the mass flow rates into or out of the liquid and vapor regions, respectively, and h_{jl} and h_{jv} are the enthalpy of the fluid entering or leaving the liquid and vapor regions, respectively. The mass of liquid m_l, mass of vapor m_v, enthalpy of liquid h_l, and enthalpy of vapor h_v are given by the following balance equations:

$$\frac{dm_l}{dt} = \sum_{jl} W_{jl},$$
$$\frac{dm_v}{dt} = \sum_{jv} W_{jv}, \tag{27}$$

$$\frac{dh_l}{dt} = \frac{1}{m_l}\sum_{jl} W_{jl}\left(h_{jl}-h_l\right) + \nu_l\frac{dp}{dt},$$
$$\frac{dh_v}{dt} = \frac{1}{m_v}\sum_{jv} W_{jv}\left(h_{jv}-h_v\right) + \nu_v\frac{dp}{dt}. \tag{28}$$

The flashing and condensation flows are given by:

$$W_f = \frac{m_l}{\Delta t}\left(\frac{h_l - h_f}{h_g - h_f}\right),$$
$$W_{\text{co}} = \frac{m_v}{\Delta t}\left(\frac{h_g - h_v}{h_g - h_f}\right). \tag{29}$$

Here Δt is the time step. The density and temperature in the downcomer is given by:

$$\rho_{\text{dw}} = \rho_{\text{dw}}(p, h_l), \tag{30}$$

$$T_{\text{dw}} = T_{\text{dw}}(p, h_l). \tag{31}$$

The level in the vessel is calculated as a function of liquid volume, that is, $N_l = N_l(V_l)$, where the liquid volume is given by $V_l = m_l\nu_l$.

An Euler method in an explicit form with a time step of 0.01 second was used to solve the ordinary differential equations of the vessel dome model.

3.6. Natural circulation loop

A natural circulation loop of the SBWR was considered in this analysis, as shown in Figure 1. Balancing the gravity head available and total loop pressure drop obtained by integration of the momentum balance leads to the model for the circulation natural. The circulation natural model includes the pressure drops and flows from the downcomer,

lower and upper plenum, reactor core, and steam separators, in order to obtain the following momentum balance:

$$\frac{dW_c}{dt} = \left(\sum_{i=1}^{n} \frac{l_i}{A_i}\right)^{-1} \left(- K_{\text{psn}} \frac{W_c^2}{\rho_{\text{dw}}} - K_{\text{sep}} \frac{W_{\text{sep}}^2}{\rho_{\text{sep}}} - \Delta p_c + \Delta p_g \right), \tag{32}$$

where $(\sum l/A)$ is the inertial term; ρ_{dw} is the downcomer density (30); ρ_{sep} is the steam-separator density; W_{sep} is the flow mass through the steam separator; K_{psn} is the support core plate loss coefficient; K_{sep} is the separator loss coefficient; Δp_c is the core pressure drop; and Δp_g is the pressure drop due to gravity.

The total core pressure drop is the sum of the frictional, acceleration, and gravitational components:

$$-\Delta p_c = \sum_{j=1}^{12} \left[\frac{\phi_{f0,j}^2 2 C_{f0} W_c^2 \Delta z}{A_{x-s}^2 D_h \rho_f} + \frac{W_c^2}{A_{x-s}^2} \left(\frac{1}{\rho_{c,j+1}} - \frac{1}{\rho_{c,j}} \right) + \rho_{c,j} g \Delta z \right], \tag{33}$$

where $j = 1, 2, \ldots, 12$ are used to indicate the core node number; C_{f0} is the single-phase friction factor; Δz_j is the core node length; D_h is the hydraulic diameter; ρ_f is the density of saturated liquid; ρ_c is the core density in each node, which is given by (5); and $\phi_{f0,j}^2$ is the two-phase multiplier given by [18]:

$$\phi_{f0}^2 = 1 + x \left(\frac{\rho_f}{\rho_g} - 1 \right), \tag{34}$$

where x is the vapor quality and ρ_g is the density of the saturated vapor.

The pressure drop due to gravity without core effects, which are considered in (32), is given by:

$$\Delta p_g = g N_l (V_l) \rho_{\text{dw}} - g (L_{\text{ps}} + L_{\text{sep}}) \rho_{\text{sep}}, \tag{35}$$

where N_l, L_{ps}, and L_{sep} are the liquid level in the vessel, the length in the upper plenum and the length in steam separators. The parameters of this model are presented in Table 7.

The Euler method in an explicit form with a time step of 0.01 second was used to solve the ordinary differential equations (ODE) of the recirculation system model.

3.7. Control models to model the control systems of SBWR

The control models obtained considering the feed water system (FW) and the main steam line (MSL) are dummy models or auxiliary models. The interface with the process at the other end of the control loop is made by the final control element. In a vast majority of nuclear engineering processes, the final control element is an automatic control valve which throttles the flow of a manipulated variable [19].

The MSL mass flow can be calculated as [19]:

$$W_{\text{ms}} = C_{v\text{ms}} f(A_{\text{ms}}^*) \Delta p_{\text{ms}} \sqrt{\frac{\rho_v}{|\Delta p_{\text{ms}}|}}, \tag{36}$$

Table 7: Circulation natural parameters.

Parameter	Value
$(\sum l/A)$	$9\,\text{m}^{-1}$
K_{psn}	$1.3\,\text{m}^{-4}$
K_{sep}	0.01m^{-4}
L_{ps}	8 m
L_{sep}	5 m
C_{f0}	0.005
Δz	0.2283 m

where $C_{v\text{ms}} = 0.4158$ is the control valve size coefficient, whose value includes the MSL system; $f(A_{\text{ms}}^*)$ is the fraction of the total flow area; A_{ms}^* is the fraction of wide open; $\Delta p_{\text{ms}} = p_{\text{Rx}} - 6.7203 \times 10^6$ is the MSL pressure drop; p_{Rx} is the reactor pressure (see Section 3.5); and 6.7203×10^6 is an estimated pressure. This equation allows reverse flow.

An analogous formulation is applied to calculate the FW mass flow:

$$W_{\text{fw}} = C_{v\text{fw}} g(A_{\text{fw}}^*) \sqrt{\rho_l \Delta p_{\text{fw}}}, \tag{37}$$

where $C_{v\text{fw}} = 0.04595$ is the control valve size coefficient, whose value includes the FW system; $\Delta p_{\text{fw}} = 7.9976 \times 10^6\,\text{Pa} - p_{\text{Rx}}$ is the feed water pressure drop; and $7.9976 \times 10^6\,\text{Pa}$ is an estimated pressure. The FW enthalpy is calculated as a function of the MSL mass flow rate, which was estimated using a typical BWR [20]:

$$\begin{aligned} h_{\text{aa}} = {} & -187903.0 + 50281.0(W_{\text{ms}}^*) - 983.3(W_{\text{ms}}^*)^2 \\ & + 8.88(W_{\text{ms}}^*)^3 - 0.03(W_{\text{ms}}^*)^4, \end{aligned} \tag{38}$$

where $W_{\text{ms}}^* = (W_{\text{ms}}/W_{\text{nom}}) \times 100$, W_{ms} is given by (43), and W_{nom} is 100% of mass flow rate. The dynamic effects are considered as a response of first-order system [19]:

$$\frac{dh_{\text{fw}}}{dt} = \frac{h_{\text{aa}} - h_{\text{fw}}}{\tau_{\text{fws}}}, \tag{39}$$

where τ_{fws} is the FW time constant. Table 8 presents the time constant.

The dynamic of the valves was modeled as a response of a first-order system:

$$\begin{aligned} \frac{dA_{\text{ms}}^*}{dt} &= \frac{S_{\text{cp}} - A_{\text{ms}}^*}{\tau_{\text{ms}}}, \\ \frac{dA_{\text{fw}}^*}{dt} &= \frac{S_{\text{cl}} - A_{\text{fw}}^*}{\tau_{\text{fw}}}, \end{aligned} \tag{40}$$

where τ_{ms} and τ_{fw} are time constants of the MS valve and FW valve, respectively; S_{cp} and S_{cl} are control signals. The time constant values are presented in Table 8.

The proportional-integral-derivative (PID) control is used for pressure control in the reactor vessel. The proportional action changes its output signal S_{cp} in direct proportion to the error signal $e_p(t)$ [19]:

$$S_{\text{cp}} = K_{\text{po}} + K_p e_p(t) + K_D \frac{de_l}{dt} + K_I \int e_p(t) dt, \tag{41}$$

Table 8: Time constant used in this work.

τ_{fws}	1000.0 s
τ_{ms}	1.25 s
τ_{fw}	10.0 s

Table 9: Control parameters.

K_{po}	0.75
K_p	18.4
K_I	18.4
K_{pl}	0.90
K_{Il}	0.02

where K_{po} is the polarization and the controller value output when there is no error; K_p, K_D, and K_I are, respectively, the proportional, derivative, and integral control gains. The tracking error is given by:

$$e_p(t) = \frac{p_{Rx} - 7.07 \times 10^6 \text{ Pa}}{p_{nom}}. \quad (42)$$

Here, p_{Rx} is the reactor pressure; 7.07×10^6 Pa is the set point of pressure; and p_{nom} is the nominal pressure. The proportional-derivative feedback control action $K_p e_p + K_D(de_l/dt)$ is used to induce certain stability margin in the controlled pressure. However, the stability of pressure does not ensure that the tracking error $e_p(t)$ can be made as small as desired. To this end, the integral action $K_I \int e_l(t)dt$, which contains the memory of the tracking error, is introduced to reduce the size of the steady-state tracking error.

The proportional-integral (PI) control is used for level control in the reactor vessel, which is given by [19]:

$$S_{cl}(t) = K_{pl}e_l(t) + K_{Il}\int e_l(t)dt, \quad (43)$$

where K_{pl} is the proportional gain; K_{Il} is the integral gain; and the tracking error is given by:

$$e_l(t) = \frac{W_{ms} - W_{fw}}{W_o} + \frac{N_{inst} - 0.97 \text{ m}}{N_o}, \quad (44)$$

where W_o is the mass flow rate; N_o is the normal level; N_{inst} is the instrument level; and 0.97 m is the set point of the level. The proportional action moves the control valve in direct proportion to the magnitude of the error, while the integral action moves the control valve based on the time integral of the error. If there is no error, the controller output does not move. As the error goes positive or negative, the integral of the error drives the controller output either up or down, depending on the action of the controller. The integral action eliminates the steady error. The control parameters used in this work are presented in Table 9.

4. RESULTS AND DISCUSSION

To demonstrate the model applicability, first, the model was validated under steady-state and transient behavior using manufacturer's predictions [20], plant data [21, 22], and RELAP5 code [23]. Afterwards, the model was applied to the SBWR to analyze steady-state conditions at 100% of the rated power and to analyze the transient behavior during the closure of all main steam line isolation valves (MSIVs). Table 2 shows the nominal values of the SBWR used in the simulation.

4.1. Validation

The qualification assessment of the simplified model is presented in Appendix. The model predictions were compared with plant data and manufacturer's predictions under steady-state behavior [20, 22]. To demonstrate the model applicability under transient behavior, an event occurred in the Laguna Verde nuclear power plant (LVNPP) was selected [21]. The plant data is compared with that obtained with RELAP5 [23] and the simplified model described in this work. The comparison results between RELAP5 and simplified model against plant data show that both computer codes have the capability to adequately predict the reactor behavior.

4.2. Steady-state behavior

Table 2 shows the nominal values of the SBWR used in the simulation. The axial power distribution in the core (Figure 3) shows a high peak value in nodes 4 and 5 that correspond to the middle part of the fuel assembly. The lower power factor corresponds to the top and bottom of the assembly, where the neutron leakage is higher. This is a quite standard profile in a BWR, but using different schemes of the control rod the axial power shape is flatted along the fuel assembly in order to decrease the hot point in case of operational transient.

Figure 5 shows the behavior of the mixture density in the core. This is one of the most important parameters for the reactor that works under natural circulation, where the differences of the density of the coolant between the top and bottom of the core establish the natural flow.

The void fraction distribution (Figure 6) along the fuel assembly corresponds to a quiet standard BWR. Here, the heat transfer to the coolant increases the void fraction 70% before the dry step.

The radial and axial temperature distribution in the fuel is shown in Figure 7. The first radial node corresponds to the surface of the fuel cladding that is keeping about 560 K by the coolant flow. This temperature is the typical value during normal operation in the standard BWR. The node 8 corresponds to the center of the fuel pellet. The higher temperature corresponds to the nodes 4 and 5 because these nodes have the higher axial power factor (see Figure 3). Figure 7 shows that the natural circulation works efficiently to cool the surface temperature, far from the thermal limit even during transient conditions as show in Section 4.3.

The change in the enthalpy from subcooled liquid to saturated liquid during the natural circulation of the liquid

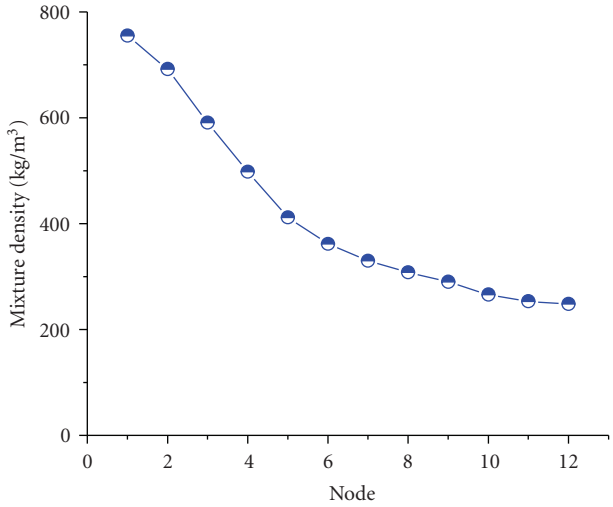

Figure 5: Axial distribution of the mixture density.

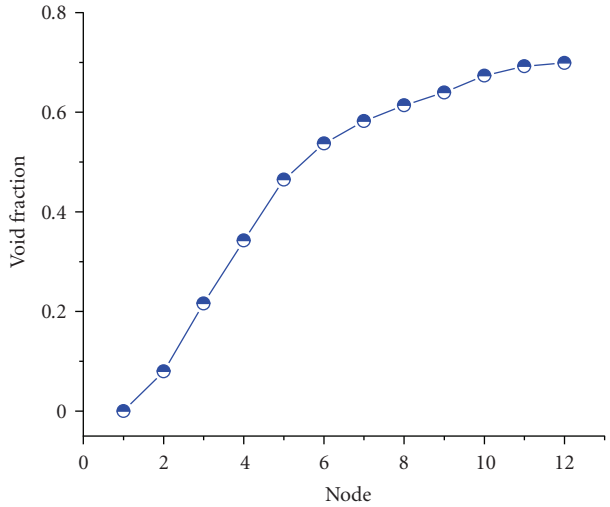

Figure 6: Axial distribution of the void fraction.

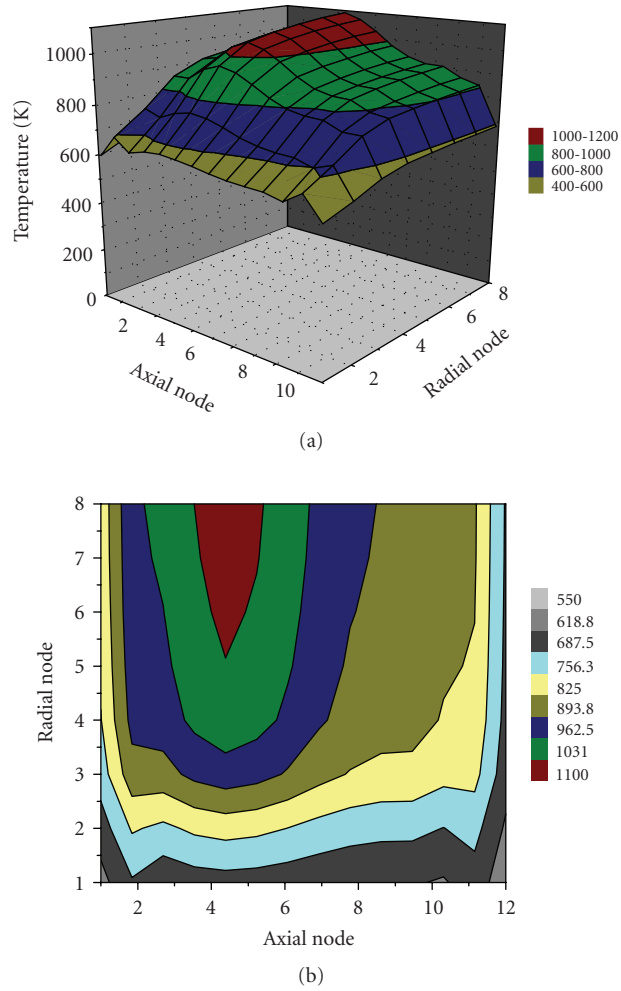

Figure 7: Fuel rod temperature distribution. (a) Surface graphic, (b) contour lines.

phase is shown in Figure 8. This effect corresponds to the heating of the coolant during its travel along the core.

The transfer of energy from the fuel to the coolant due to heat transfer increases the enthalpy of the mixture node by node as shown in Figure 9. When $h_f < h_m$, two-phase saturated exist, this takes place approximately at core node 3. If $h_m < h_f$ and $h_l < h_f$, liquid phase occurs in the core node 1, and subcooled boiling appears in the core nodes 2 and 3, respectively.

Figure 10 shows the convective heat transfer coefficient. The drastic increment of this parameter in the bottom of the core shows the importance of this mechanism to remove heat from the nuclear fuel during natural circulation. Specifically, in node 1, there is heat transfer in single liquid phase, and in nodes 2, 3, and 4 the heat transfer is governed by subcooled boiling. For the rest of the nodes the heat transfer regime is nucleate boiling.

The superficial velocity of the gas and liquid is shown in Figures 11 and 12, respectively. The superficial velocity of the gas increases due to the heating of the liquid following the curve of the void fraction. Therefore, the superficial velocity of the liquid tends to go down.

4.3. Closure of MISVs

The analysis of this transient assumes normal functioning of plant instrumentation and controls plant protection and reactor protection systems (RPSs). The sequence of the events of this transient is presented in Table 10.

The main steam isolation valves start to close in the first second with a delay of 3 seconds before closing completely, and the position switches on the valves initiate a reactor scram when the valves are less than 90% open. According to the behavior shown in Figures 13 and 14, the closure of these valves inhibits steam flow to the feed water turbines terminating feed water flow. Mitigation of pressure increase is accomplished by initiation of the reactor scram via MSIV position switches and the protection system (Figure 15) and

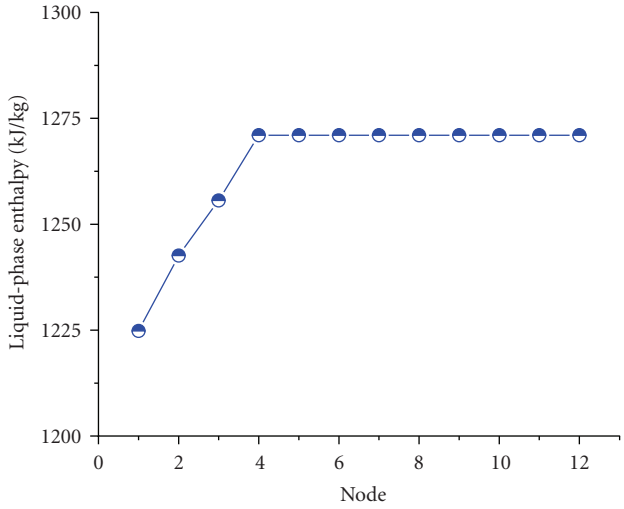

Figure 8: Axial distribution of the enthalpy of the liquid.

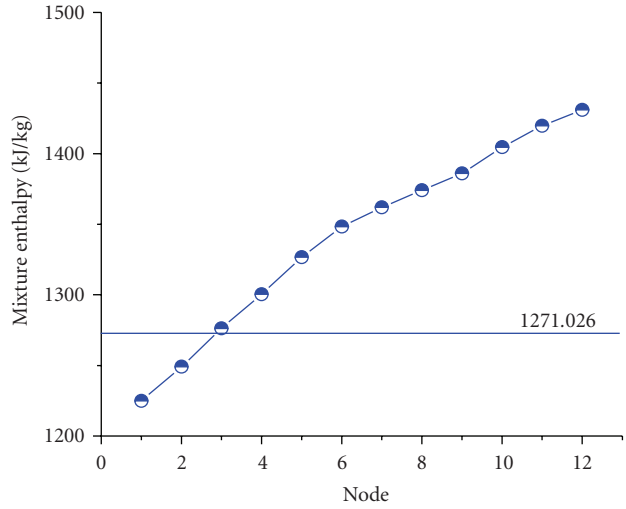

Figure 9: Axial distribution of the mixture. h_f (= 1271026) liquid saturated enthalpy.

Table 10: Sequence of events of closure of main steam isolation valves.

Elapsed time (sec.)	Event
0.0	Reactor under steady-state condition rate at full power.
1.0	Closure of all main steam isolation valves.
2.0	Maximum power peak is reached (120% of rated).
2.0	The peak of pressure is maximum, and the SRVs opening to relief pressure.
2.0+	Reactor lever decreases until the emergency core cooling system actuation.
10.0+	Core flow tend to stabilize at new equilibrium conditions (natural circulation).

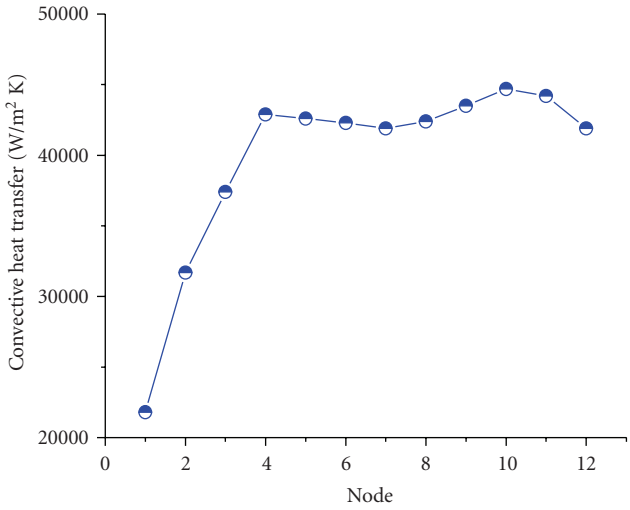

Figure 10: Axial distribution of the convective heat transfer during natural circulation.

the opening of the safety relief valves (SRVs) to limit system pressure (Figure 16). The peak of thermal power reaches 120% of rated power after approximately 3 seconds as shown in Figure 15, which is due to the drastic reduction of the void fraction in the core (Figure 17). This peak of power is limited by the set point scram at 118% of neutronic power. The peak pressure will still remain considerably below the ASME code limit of 1375 psig (9.48 MPa) as shown in Figure 18. The loss of feed water flow produces a reduction in the water lever in the reactor vessel as shown in Figure 19; the initiation of the emergency core cooling systems (ECCSs) occurs at approximately 33 seconds after detection; and the low level is not shown here. The scram of the reactor causes a reduction of the core flow (Figure 20). Figure 21 shows the heat transfer from the fuel to the coolant, where the shape follows the scram curve.

Figure 22 shows the behavior of the core flow in respect to void fraction. After the closure of the MISVs, the void fraction decreases suddenly due to pressure raise in the reactor vessel, which produces unbalance between the gravity head and the total loop pressure drop; therefore, the core flow decreases. This decrease can be observed in the figure, where finally the core flow reaches 70% of the rated core flow with 20% of the rated void fraction. This behavior is very important to core cooling. Figure 23 shows the neutronic power behavior in respect to core flow. In general terms, this figure shows that after shutdown the core flow keeps maintaining high values for low power values, which must guarantee the core cooling due to residual heat. The expanded graphic (Figure 23) shows that at the maximum power level the core flow increases slightly as expected.

5. CONCLUSIONS

A simplified model for transient analysis on boiling water reactor (BWR) working with natural circulation is described

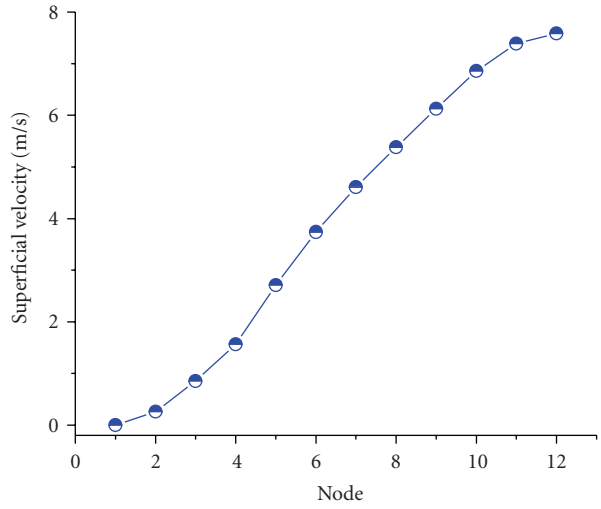

Figure 11: Superficial velocity for the gas phase.

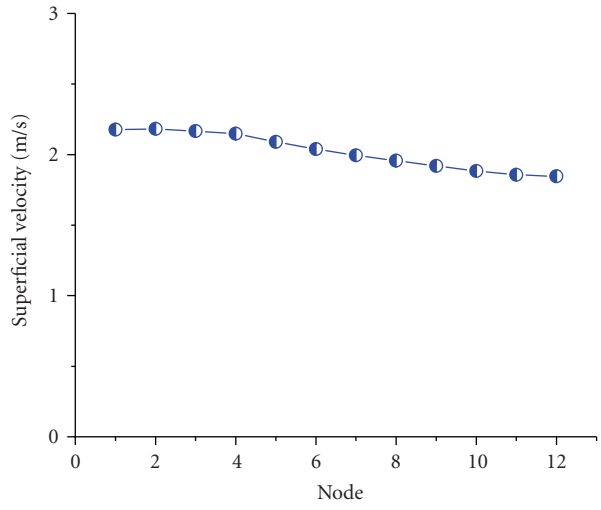

Figure 12: Superficial velocity for the liquid phase.

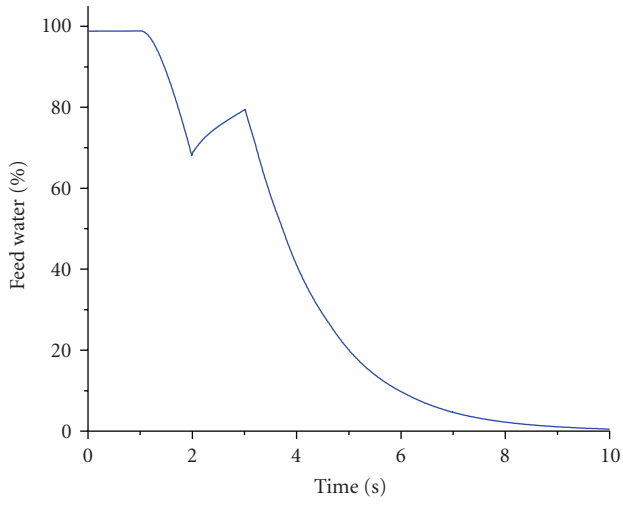

Figure 13: Feed water behavior.

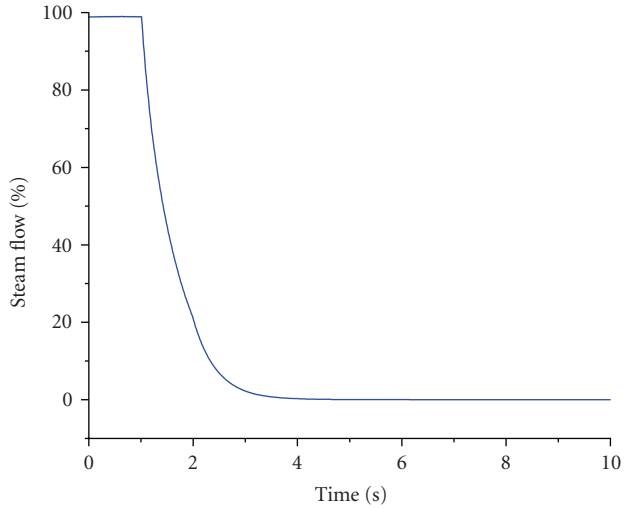

Figure 14: Steam flow behavior.

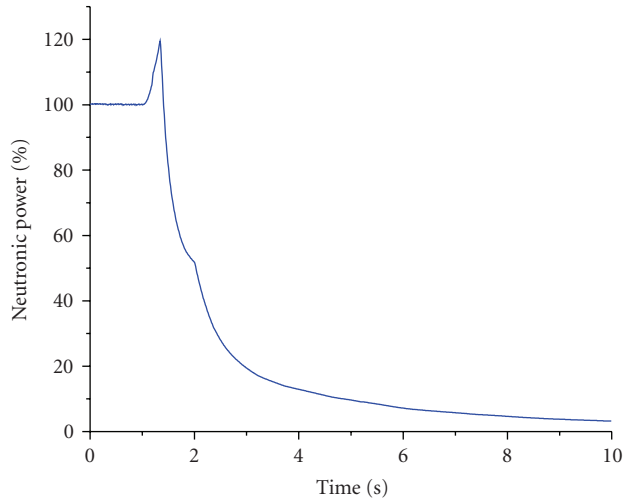

Figure 15: Neutronic power behavior during the closure of MSIVs.

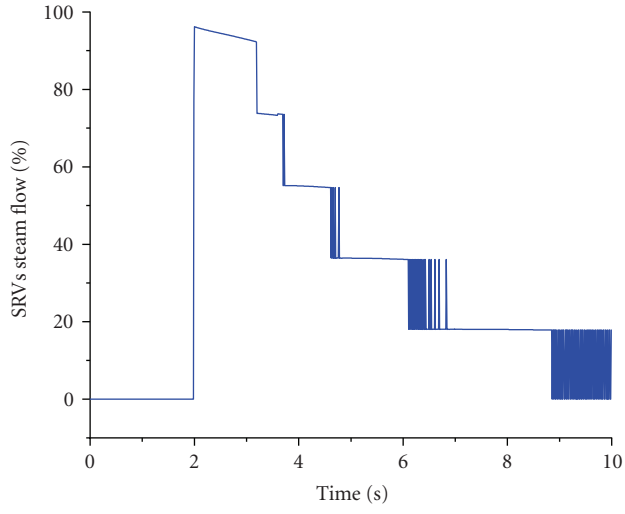

Figure 16: SRV'S steam flow by closure of MSIVs.

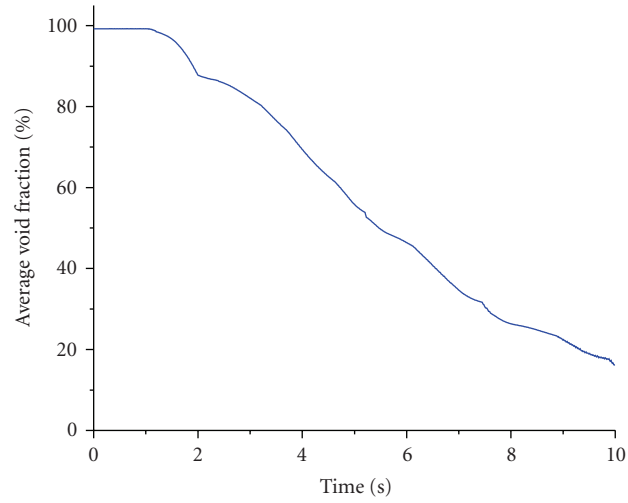

Figure 17: Average void fraction behavior.

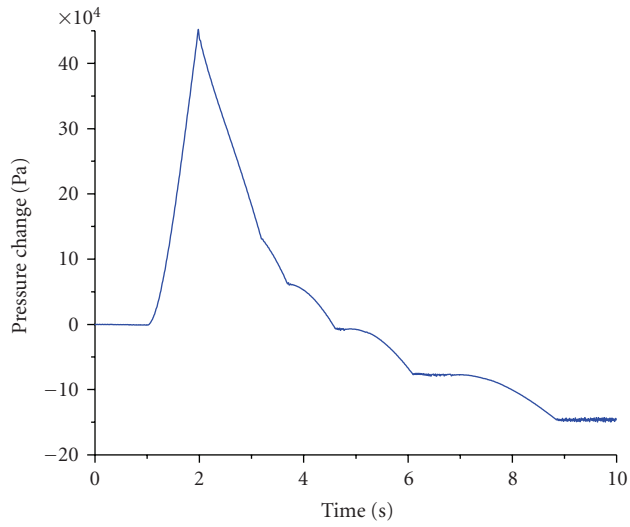

Figure 18: Pressure change in the dome of the reactor vessel.

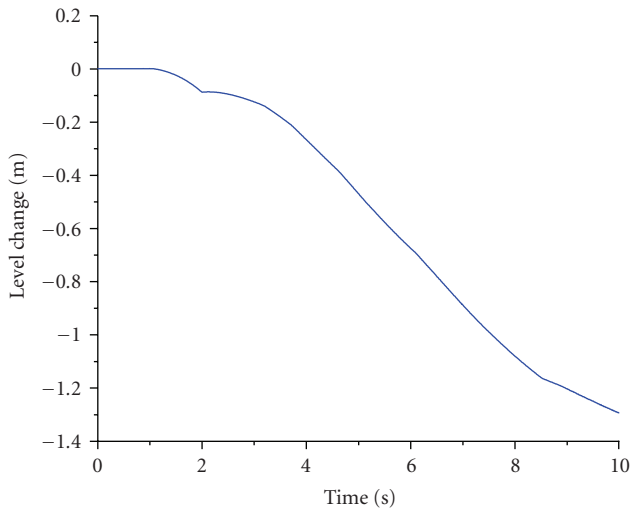

Figure 19: Water lever reduction due to loss of feed water.

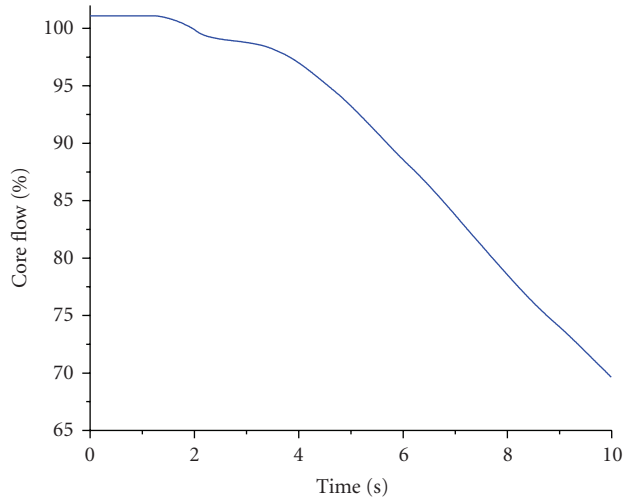

Figure 20: Core flow behavior.

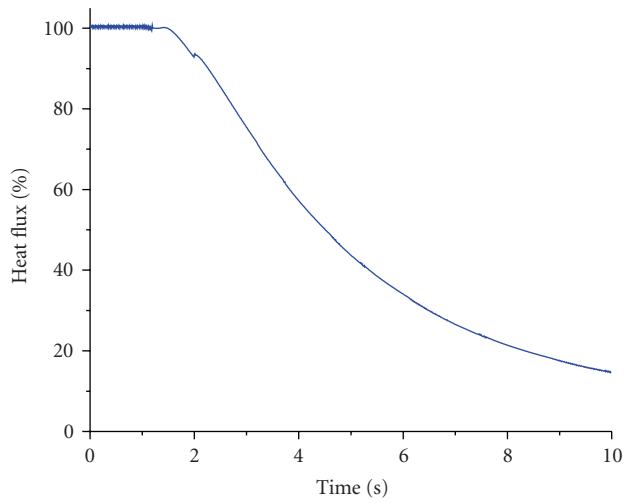

Figure 21: Heat flux behavior.

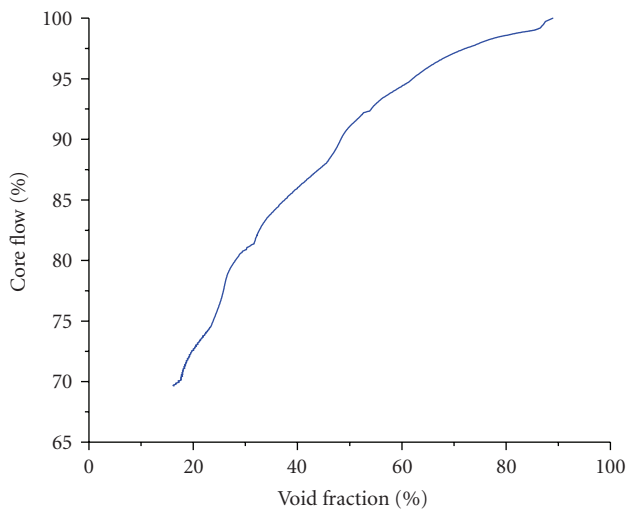

Figure 22: Core flow versus void fraction.

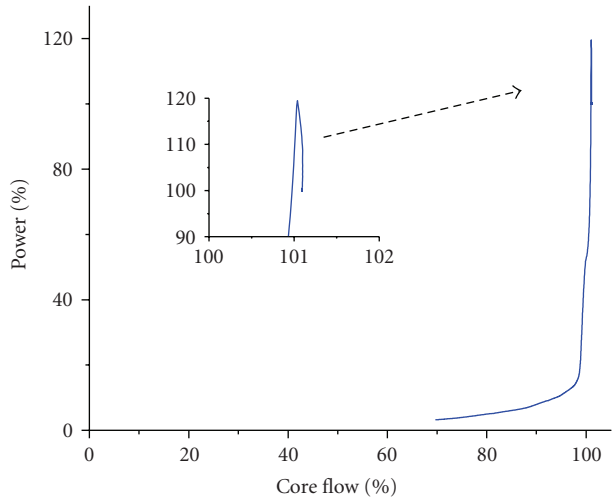

Figure 23: Neutronic power versus core flow.

in this paper. This model was based on lumped and distributed parameter approximations, which includes vessel dome and downcomer, neutron kinetics, fuel temperature, lower and upper plena reactor core, and pressure and level controls.

The steady state and the transient of closure of main steam valves were presented and analyzed. The numerical results obtained with the model show a behavior physically consistent both in steady-state and transient behavior. Appendix A is a comparison of the simplified model predictions with plant data, manufacturer's predictions, and RELAP5 under steady-state and transient conditions, showing good predictions between plant data and codes calculations. Therefore, the simplified model described in this paper provides reliable results to predict the behavior of a BWR working with natural circulation under normal and abnormal conditions.

Our results in the transient of closure of main steam valves show that the cooling system due to natural circulation in the SBWR is around 70% of the rated core flow. This can guarantee the core cooling due to residual heat.

Natural convection circulation of coolant in the reactor cooling system is used to some extent in all the reactor concepts, and many of these uses are innovative. Therefore, the need is to develop or confirm the design basis and to develop and qualify computer codes to enable reliable safety analysis.

Simplified model as shown in this work can be used to predict phenomena on SBWR behavior during the evaluation of the safety of a nuclear power plant which requires analysis of the plant's responses to postulate equipment failures or malfunctions. Such analysis helps to determine the limit conditions for operation, limit safety system settings, and design specifications for safety-related components and systems to protect public health and safety.

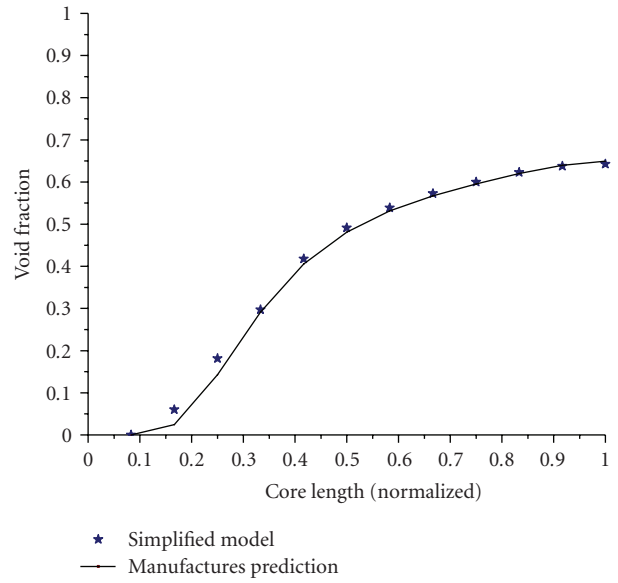

Figure A.1: Profile of the void fractions in comparison with manufacturer's predictions [20].

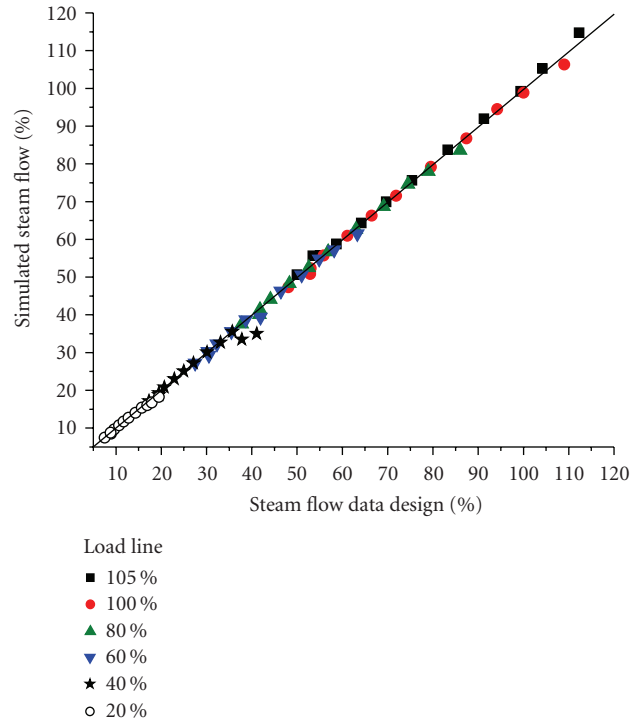

Figure A.2: Steam flow comparison with data design [22].

APPENDICES

A. QUALIFICATION ASSESSMENT FROM STEADY STATE

The profile of the void fraction prediction was compared with the manufacturer's predictions [20]. The numerical results obtained with the simplified model show that void

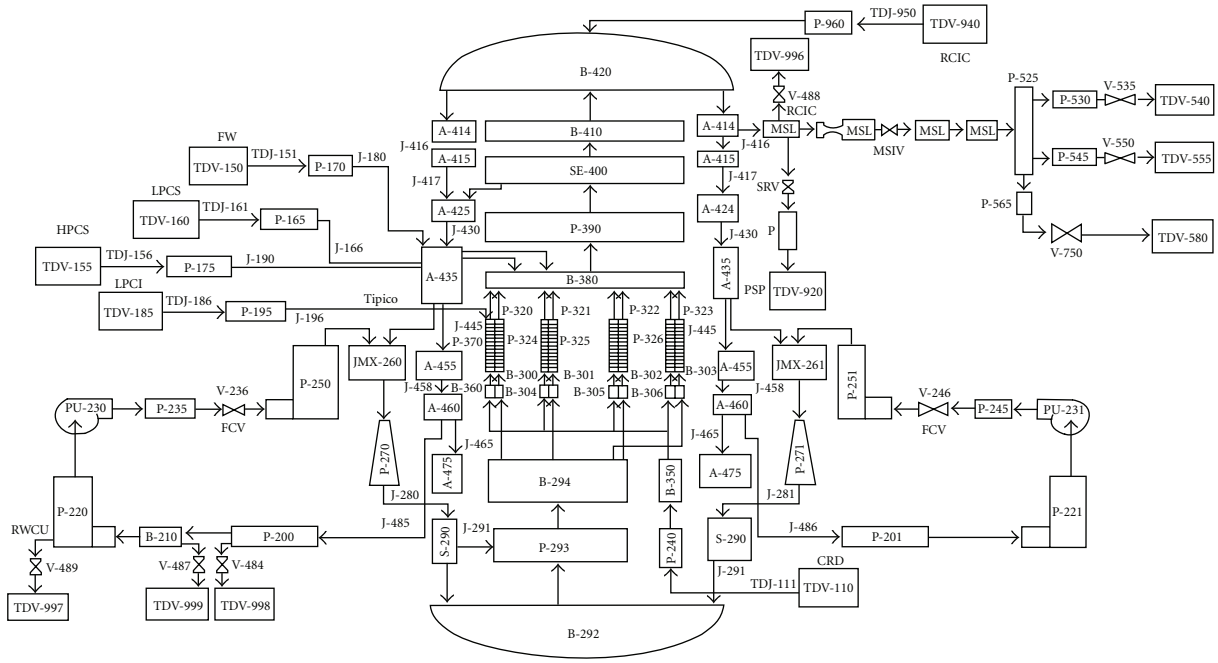

Figure A.3: Nodalization of Laguna Verde nuclear power plant with RELAP5 [21].

fraction behavior is similar to the results reported by the final safety analysis report [20] for a typical BWR. This assessment is shown in Figure A.1. In this figure, it can be observed that manufacturer's results underpredict the void fraction in the subcooled boiling region (approximated of 0.15 to 0.35 of core length). After this region, the profile is predicted with an accuracy of 0.323%.

The steam flow data design [22] in the reactor for a typical BWR is predicted with a maximum accuracy of 2.4%. This assessment is shown in Figure A.2 for different load lines.

B. QUALIFICATION ASSESSMENT OF THE SIMPLIFIED MODEL UNDER TRANSIENT CONDITIONS

For the validation of the model under transient conditions, a transient occurred in the Laguna Verde nuclear power plant (LVNPP) was selected [21]. The plant data is compared with those obtained with RELAP5 [23] and the simplified model described in this work. This transient occurred in LVNPP Unit 2 on June 25th 1999, during the maintenance activities in the filters of the reactor water cleanup system (RWCU). A wrong sequence in the opening of valves of the RWCU caused a differential pressure and small pieces of the filter going up inside the reactor vessel. The signal of high radiation in the main steam lines causes a reactor SCRAM. This transient occurs at 90% of the full power.

Figure A.3 shows the nodalization diagram of the LVNPP for the RELAP5 computer code. This is a typical boiling water reactor 5. In this model, the feed water, turbine, suppression pool, control rod drive system, and emergency cooling systems are represented by boundary conditions. Four fuel rod channels represent the core of the reactor [23].

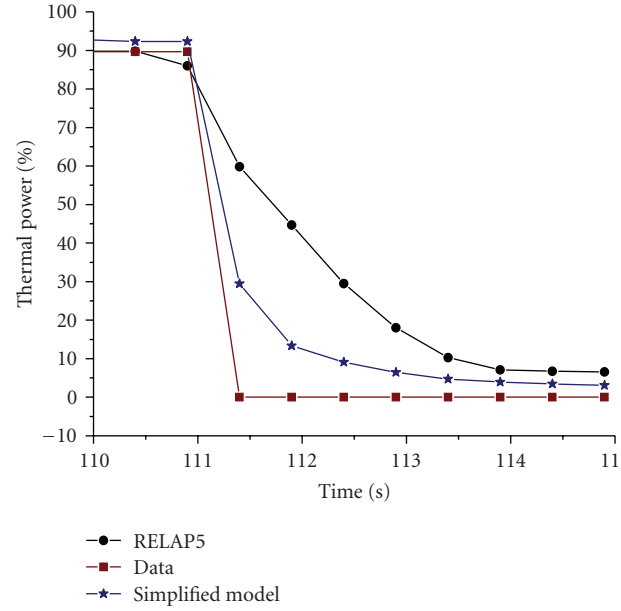

Figure B.4: Thermal power behavior during the shutdown of the reactor.

The signal of high radiation in the main steam lines causes the scram of the reactor and this is shown in Figure B.4. This Figure shows a comparison among plant data, RELAP5, and simplified model results. The prediction of the simplified model is between RELAP5 calculation and plant data.

The pressure of the reactor vessel is shown in Figure B.5. The maximum peak of pressure according to the plant data

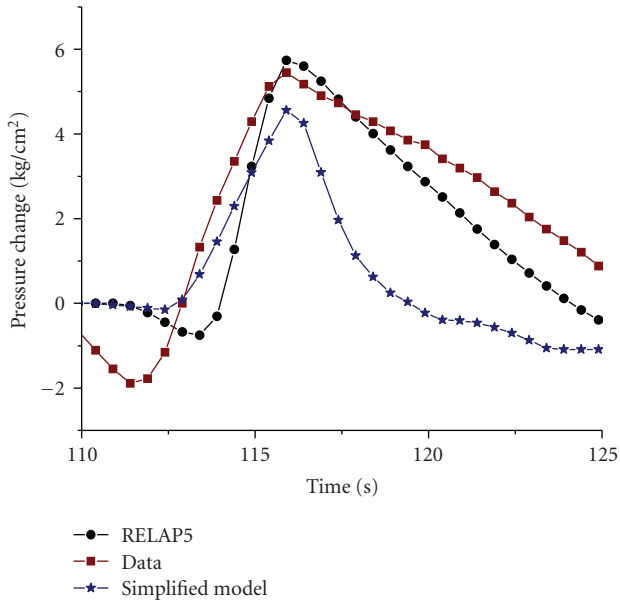

Figure B.5: Pressure rise of the reactor due to closure of main steam valves.

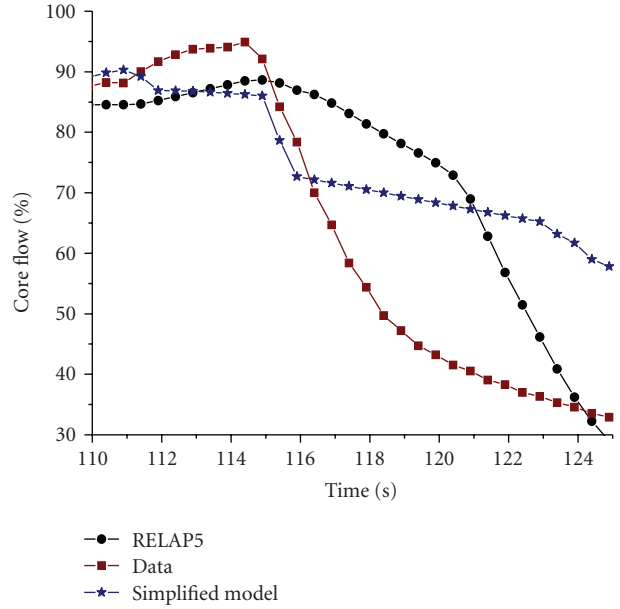

Figure B.6: Core flow reduction by recirculation pump trip.

is 75.69 Kg/cm^2, and the simplified model shows an error of 2.5% below that value. RELAP5 calculation shows that the peak of pressure is well predicted. The opening of the safety relief valves causes a fast reduction of the pressure. In the simplified model, this reduction is slower than RELAP5 prediction.

The core flow reduction due to the trip of the recirculation pumps by high pressure in the reactor vessel is shown in Figure B.6. In this case, RELAP5 and the simplified model overpredicts the core flow, but during the first 5 seconds of the transient the results obtained with the simplified model

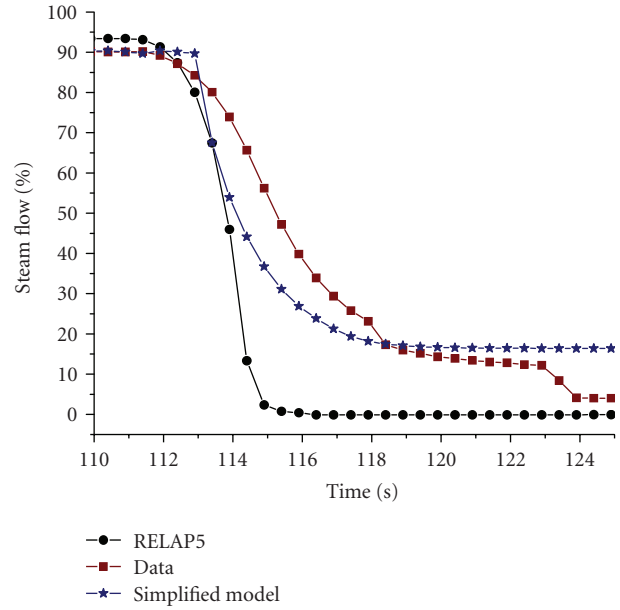

Figure B.7: Steam flow reduction during the closure of main steam valves.

are closer to the plant data, with a maximum difference of 12%.

Figure B.7 shows the behavior of the steam flow. Again, the prediction of the simplified model is between plant data and RELAP5 calculation. The highest difference during the first 5 seconds of the transient is lower than 3%.

The comparison results between RELAP5 and simplified model against plant data shows that both computer codes have the capability to adequately predict the reactor behavior. One of the main advantages of the simplified model is that it spends less time to simulate different transients with a high reliability in results.

NOMENCLATURE

a, b, c, d: Coefficients (see (24))
A^*_{fw}: Fraction of wide open of the FW control valve
A^*_{ms}: Fraction of wide open of the MSL control valve
A_{x-s}: Cross-sectional area (m^2)
c_i: Delayed neutron concentration
C_o: Distribution parameter
C_{f0}: Single-phase friction factor
C_{vfw}: FW control valve-size coefficient (m^2)
C_{vms}: MSL control valve-size coefficient (m^2)
Cp_l: Liquid specific heat (J/kg·K)
D_h: Hydraulic diameter (m)
$e_p(t)$: Error signal
F: Convective boiling factor
$F(z)$: Axial power factor
f: Friction factor
G: Mass flux (kg/s·m^2)
H_o: Condensation parameter (1/s·K)
H_∞: Convective heat transfer coefficient (J/s·m^2·K)

h: Enthalpy (J/kg)
h_{fg}: Difference in specific enthalpy between saturated vapor and liquid (J/kg)
h_l: Liquid enthalpy (J/kg)
h_v: Vapor enthalpy (J/kg)
j: Superficial velocity (m/s)
K_D: Derivative control gain (s)
K_I: Integral control gain (s^{-1})
K_{Il}: Integral gain (s^{-1})
K_p: Proportional control gain
K_{pl}: Proportional gain
K_{po}: Polarization
K_{psn}: Support core plate loss coefficient (m^{-4})
K_{sep}: Separador loss coefficient (m^{-4})
k_l: Liquid thermal conductivity (J/s·m·K)
L_{ps}: Length in the upper plenum (m)
L_{sep}: Length in the steam separators (m)
m_l: Mass of liquid (kg)
m_v: Mass of vapor (kg)
$n(t)$: Normalized neutron flux
N_{inst}: Instrument level (m)
N_l: Liquid level in the vessel(m)
N_o: Normal level(m)
P_0: 100% of rated power(J/s)
P_H: Heated perimeter(m)
p_{Rx}: Reactor pressure(Pa)
p: Pressure (Pa)
q'': Heat flux (J/s·m^2)
q''': Volumetric heat generation by gamma radiation(J/s·m^3)
S_{cp}: Output signal
$\langle T_f \rangle$: Average fuel temperature(K)
T_m: Moderator temperature(K)
T_s: Saturation temperature(K)
v_{gj}: Average drift velocity(m/s)
W_o: 100% of rated of the mass flow(kg/s)
W_c: Core mass flow rate(kg/s)
W_{gin}: Gas mass flow rate (kg/s)
W_{jl}: Liquid mass flow rate (kg/s)
W_{jv}: Vapor mass flow rate (kg/s)
W_{lin}: Liquid mass flow rate (kg/s)
W_{nom}: 100% of mass flow rate (kg/s)
W_{sep}: Mass flow rate through the steam separator (kg/s)
x: Vapor quality
X_{tt}: Martinelli factor.

GREEK SYMBOLS

β: Neutron delay fraction
β_i: Portion of neutrons generated by the ith group
Γ: Volumetric vapor generation rate (kg/m^3)
Δp_c Core pressure drop (Pa)
Δp_g: Drop pressure due to gravity (Pa)
Δt: Time step (s)
Δz: Cell length in axial direction (s)
ε_g: Void fraction
Λ: Neutron generation time (s)
ρ: Density (kg/m^3)
ρ_c: Core density in each node (kg/m^3)
ρ_D: Doppler effect (pcm)
ρ_{dw}: Downcomer density (kg/m^3)
ρ_{cr}: Reactor control rods (kg/m^3)
ρ_f: Density of saturated liquid (kg/m^3)
ρ_g: Density of the saturated vapor (kg/m^3)
ρ_m: Rmoderador temperature reactivity (pcm)
ρ_{sep}: Steam-separator density (kg/m^3)
τ_v: Void fraction reactivity (pcm)
$(\sum l/A)$: Inertial term (m^{-1})
τ_{fws}: Time constant of the FW enthalpy (s)
τ_{ms}: Time constant of the MS valve (s)
τ_{fw}: Time constant of the FW valve (s)
$\phi^2_{f0,j}$: Two-phase multiplier.

SUBSCRIPTS

f: Fuel, saturated liquid
g: Gas phase
l: Liquid phase
m: Mixture in two-phase flow.

ACKNOWLEDGMENTS

The authors are grateful to Erick Gilberto Espinosa-Martínez for assistance provided during this study. Additional thanks are also due to the reviewers of the paper whose comments and observations helped to improve it substantially.

REFERENCES

[1] Nuclear Energy Agency (NEA), "Innovative nuclear reactor development, opportunities for international co-operation," Paris, France, 2002.
[2] J. Lillington, *The Future of Nuclear Power*, Elsevier, Amsterdam, The Netherlands, 2004.
[3] IEA/OECD (NEA)/IAEA, "Innovative nuclear reactor development: opportunities for internacional co-operation," 2002.
[4] Y. Zhang, D. Zhang, and D. Dong, "Analysis of the nuclear heating reactor and its possible application in seawater desalination," IAEA-TECDOC-1056, November 1998.
[5] IAEA-TEC-DOC-1289, "Comparative assessment of thermophysical and thermodraulic characteristics of lead, lead-bismuth and sodium coolant for fast reactors," Vienna, Austria, 2002.
[6] IAEA-TECDOC-968, "Status of advanced light water cooled reactor design 1996," September 1997.
[7] IAEA-TECDOC-968, "Utility requirements and safety objectives for advanced water cooled reactors, status of advanced light water cooled reactor designs 1996," September 1997.
[8] W. X. Tian, S. Z. Qui, Y. Guo, H. G. Su, and D. N. Jia, "Development of a termal-hydraulic analysis code for CARR," *Annals of Nuclear Energy*, vol. 32, no. 3, pp. 261–279, 2005.
[9] "Design characteristics of SBWR," 2007, http://www.nuc.berkeley.edu/designs/sbwr/char.html.
[10] N. Zuber and J. A. Findlay, "Average volumetric concentration in two-phase flow systems," *Journal of Heat Transfer*, vol. 87, pp. 453–468, 1965.

[11] R. T. Lahey, "A mechanistic subcooled boiling model," in *Proceedings of the 6th International Conference on Heat Transfer*, Toronto, Ontario, Canada, August 1978.
[12] P. Saha and N. Zuber, "Point of net vapor generation and vapor void fraction in subcooled boiling," in *Proceedings of the 5th International Conference on Heat Transfer*, Tokyo, Japan, September 1974.
[13] J. H. L. Duderstadt, *Nuclear Reactor Analysis*, John Wiley & Sons, New York, NY, USA, 1976.
[14] W. Wulff, H. S. Cheng, S. V. Lekach, and A. N. Mallen, "The BWR plant analyzer," NUREG/CR-3943, BNL-NUREG-51812, 1984.
[15] S. V. Patankar, *Numerical Heat Transfer and Fluid Flow*, McGraw-Hill, New York, NY, USA, 1980.
[16] F. W. Dittus and L. M. Boelter, "Heat transfer in automobile radiators of the tubular type," *University of California Publications in Engineering*, vol. 2, pp. 443–461, 1930.
[17] J. C. Chen, "A correlation for boiling heat transfer to saturated fluid in convective flow," 63-HT-34. American Society of Mechanical Engineers, 1963.
[18] G. B. Wallis, *One Dimensional Two-Phase Flow*, McGraw-Hill, New York, NY, USA, 1969.
[19] W. L. Luyben, *Process Modeling, Simulation and Control for Chemical Engineers*, McGraw-Hill, Singapore, 1990.
[20] Comisión Federal de Electricidad, "Final Safety Analysis Report," Central Laguna Verde Unit 1, Mèxico DF, 1979.
[21] R. Hernanadez-Garcia, "Simulación del Transitorio "Aislamiento de Líneas Principales de Vapor Por Señal de Alta-Alta Radiación"," B.s. thesis, Universidad Autónoma Metropolitana-Iztapalapa, México DF, Mexico, 2006.
[22] Comisión Federal de Electricidad, "Laguna Verde Unit 1," Proprietary information, 1990.
[23] "RELAP5/MOD3 Code Manual, Models and Correlations," NUREG/CR-5535, Volume 4, USNRC, 1995.